Available online at www.sciencedirect.com
ScienceDirect
Trans. Nonferrous Met. Soc. China 32(2022) 790−800
Transactions of Nonferrous Metals Society of China
www.tnmsc.cn

Microstructure and mechanical properties of 6082 aluminum alloy processed by preaging and hot forging

Lin HUA[1,2,3,4], Pu-guang YUAN[1,2], Ning ZHAO[1,2], Zhi-li HU[1,2,3,4], Hui-juan MA[1,2]

1. Hubei Key Laboratory of Advanced Technology for Automotive Components, Wuhan University of Technology, Wuhan 430070, China;
2. Hubei Collaborative Innovation Center for Automotive Components Technology, Wuhan University of Technology, Wuhan 430070, China;
3. Hubei Research Center for New Energy & Intelligent Connected Vehicle, Wuhan University of Technology, Wuhan 430070, China;
4. Hubei Engineering Research Center for Green & Precision Material Forming, Wuhan University of Technology, Wuhan 430070, China

Received 22 March 2021; accepted 29 October 2021

Abstract: A novel forging process of 6082 aluminum alloy is proposed, which can save time and reduce energy consumption while ensuring mechanical properties. In this process, the billet was preforged at solid solution temperature and then preaged, followed by warm forging at 200 °C. The flow behavior of the preaged samples during compression and the mechanical properties of the formed samples were investigated by hot compression tests. The differences in the precipitated phases of the samples with different processing parameters were analyzed by scanning electron microscopy (SEM), transmission electron microscopy (TEM), and differential scanning calorimetry (DSC). The best comprehensive performance was obtained after preaging at 120 °C for 4 h and holding at 200 °C for 10 min, and the Vickers hardness was HV 128, which was higher than that of the traditional process. Precipitation strengthening and dislocation strengthening were improved when the samples were formed at 200 °C. This forging process shows the advantages of short time consumption and low energy consumption, which can effectively improve the production efficiency while ensuring the strength after forming.

Key words: 6082 aluminum alloy; forging; preaging; compression behavior; hardness; precipitates

1 Introduction

Lightweighting of automobiles is an important way to reduce automobile emissions. 6082 Al alloy, as a typical lightweight material [1], has good formability, strength, toughness, and corrosion resistance [2], and is widely used in hot forging manufacturing of automobile chassis parts [3,4].

The traditional hot forging process of 6082 aluminum alloy is as follows. The billet is heated to 450 °C for large-deformation preforging to form the initial geometric shape and then transferred to the final forging die for final forging to complete the detailed deformation followed by edge cutting treatment to obtain the desired shape. After forming, solid solution treatment at 535 °C for 1.5 h and artificial aging at 180 °C for 8 h are carried out to ensure satisfactory mechanical properties. A large number of scholars have researched the forging process. BIROL and ILGAZ [5] produced suspension parts using the above process of forming at 450 °C, solid solution treatment at 535 °C, and aging for 8 h. To reduce energy consumption and

Corresponding author: Zhi-li HU, E-mail: zhilihuhit@163.com
DOI: 10.1016/S1003-6326(22)65833-3

improve production efficiency, BIROL et al [6] studied the properties and microstructure of 6082 aluminum alloy forged without postforming solid solution process, and with only artificial aging. It was concluded that by combining the solid solution treatment and forging into one process, energy savings and efficiency improvement were achieved. To improve the efficiency of artificial aging, DIN et al [7] studied the mechanical properties and microstructure of an Al−Mg−Si alloy treated by different heat treatment methods, including solid solution treatment and subsequent artificial aging (T6 treatment) and solid solution treatment followed by cold working and artificial aging (T8 treatment). It was found that applying cold working between solid solution treatment and artificial aging can accelerate the precipitation, resulting in higher mechanical properties of the alloy and less peak aging time. However, cold deformation might lead to forging cracks and reduce the fatigue performance due to local stress concentrations, resulting in the narrow applicability of this process [8].

In the view of the above problems, a new forging process was proposed in this work, which included solid solution treatment, preforging, aging and final forging, as schematically shown in Fig. 1. By applying the proposed process, the postforging solid solution treatment was omitted. The low-temperature preaging of the forgings after preforging reached the underaged state. Peak aging was performed by medium-temperature preservation before final forging. To verify the feasibility of the proposed process, the flow behavior of preaged samples, mechanical properties, and microstructure of samples after isothermal compression were investigated. To reveal the reasons for the difference in mechanical properties among different samples, the relationship between mechanical properties and microstructure was studied, and the relationship among grain structure, dislocation, precipitate, and mechanical properties was analyzed.

2 Experimental

The composition of 6082 aluminum alloy is given in Table 1. The 6082 aluminum alloy material was cut into cylinders of 10 mm in diameter and 15 mm in height by a wire-cut machine.

6082 aluminum alloy samples were compressed on a DATA SCIENCES INTERNATIONAL Gleeble 3500 testing machine. To enhance the thermal conductivity, tantalum plates were added at both ends of the sample. In this experiment, the heating rate was 5 °C/s, and the strain rate was 1 s^{-1}. The solid solution treatment was performed at 535 °C for 30 min, after which preaging was

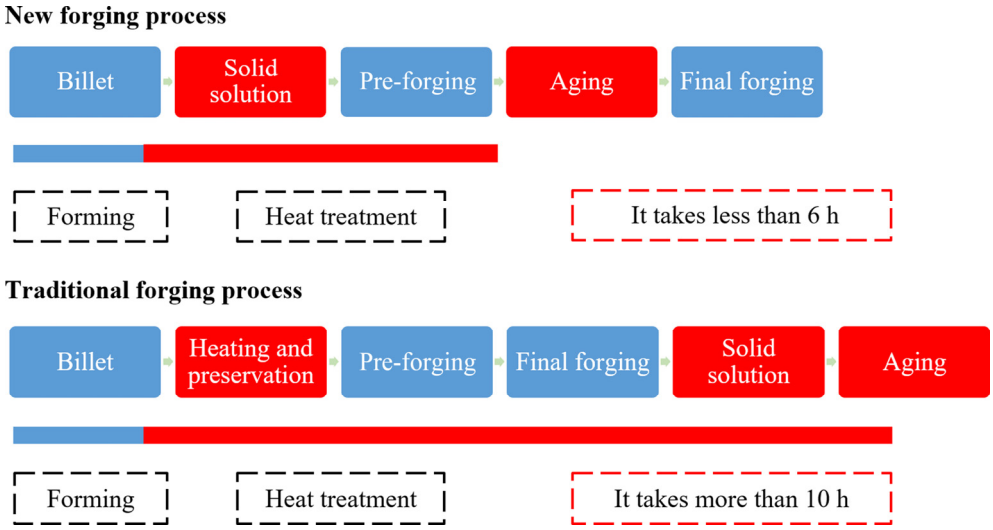

Fig. 1 Comparison of new process and traditional process

Table 1 Composition of 6082 aluminum alloy sample (wt.%)

Si	Fe	Cu	Mn	Mg	Cr	Zn	Ti	Al
0.95	0.18	0.06	0.45	0.65	0.12	0.005	0.1	Bal.

conducted at 120 °C for 2, 4 and 6 h followed by constant temperature holding before compression at 200 and 250 °C for 5 and 10 min, and the samples were quenched to room temperature immediately after compression. To compare the difference between the preaging process and the natural aging process (T4 treatment), the T4-treated sample was also tested, which was aged at room temperature for 96 h, as shown in Fig. 2.

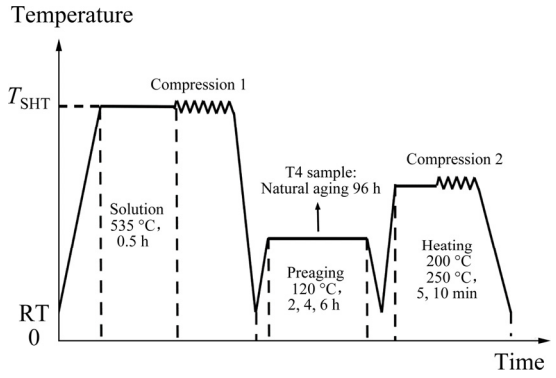

Fig. 2 Time−temperature curves of samples

The flow behavior was tested by a Gleeble 3500 testing machine. The heating rate was 5 °C/s, and isothermal compression was carried out after heating to the deformation temperature. The Vickers hardness of the samples was tested by a Huayin HV−1000A Vickers hardness tester. The indenter pressure was 200 g, and the holding time was 10 s. At least ten points at different positions were selected for each measuring sample, and the average value of ten measured results was taken as the hardness of the sample. The area of Vickers hardness test is shown in Fig. 3. A German Netzsch STA449F3 synchronous thermal analyzer was used to perform differential scanning calorimetry (DSC) experiments. At a heating rate of 10 °C/min, the temperature rose from room temperature to 550 °C, and the DSC curves of heat absorption and heat release were recorded. The microstructure of the samples was observed by a Zeiss Axio Scope A1 optical microscope (OM), and the characterization position for microstructure is shown in Fig. 3. An FEI QUANTA 450 SEM was used to observe the amount and distribution of precipitates. Transmission electron microscopy (TEM) was conducted by a JEM−1400plus TEM to observe the morphology of precipitates of the samples, which were twin-jet electropolished at −25 °C with a mixture of 30% HNO_3 and 70% CH_3OH after being mechanically polished to a thickness of 0.04 mm.

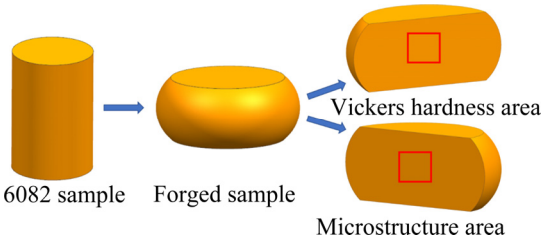

Fig. 3 Characterization position for microstructure and HV tests

3 Results

3.1 Compression behavior after pretreatment

Figure 4 shows the true strain−stress curves of isothermal compression under conditions of different temperatures and different holding time. This behavior represents the compression behavior of aluminum alloys, and compression behavior is very important for the forming behavior of aluminum alloys [9]. When the deformation temperature is 200 °C and the holding time is 5 min, the compressive strength is 250−290 MPa (Fig. 4(c)). When the holding time is 10 min (Fig. 4(a)), the sample has the most compressive strength with a maximum value of 328 MPa. When the deformation temperature rises to 250 °C and the holding time is 5 min (Fig. 4(d)), the compressive strength is 140−150 MPa. When the holding time is 10 min (Fig. 4(b)), the compressive strength is 130−160 MPa. The results show that the plasticity at 250 °C is better than that at 200 °C, and the metal softens more fully with increasing temperature. The flow behavior of samples during hot compression can be used to obtain the deformation resistance with different parameters [10], and the load of final forging at 250 °C is lower than that at 200 °C. According to the trend of isothermal compression true strain−stress curves, when the strain reaches a certain level, the work hardening and softening reach dynamic equilibrium and the curve tends to be stable [11]. Since the deformation temperature of samples is below recrystallization temperature [12], the softening mechanism can be judged as dynamic recovery [13]. The compressive strength of the T4-treated sample (Fig. 4(e)) compressed at 200 and 250 °C is similar to that of the sample compressed at 200 °C after preaging. When the temperature rises to 300 °C, softening phenomenon is also observed.

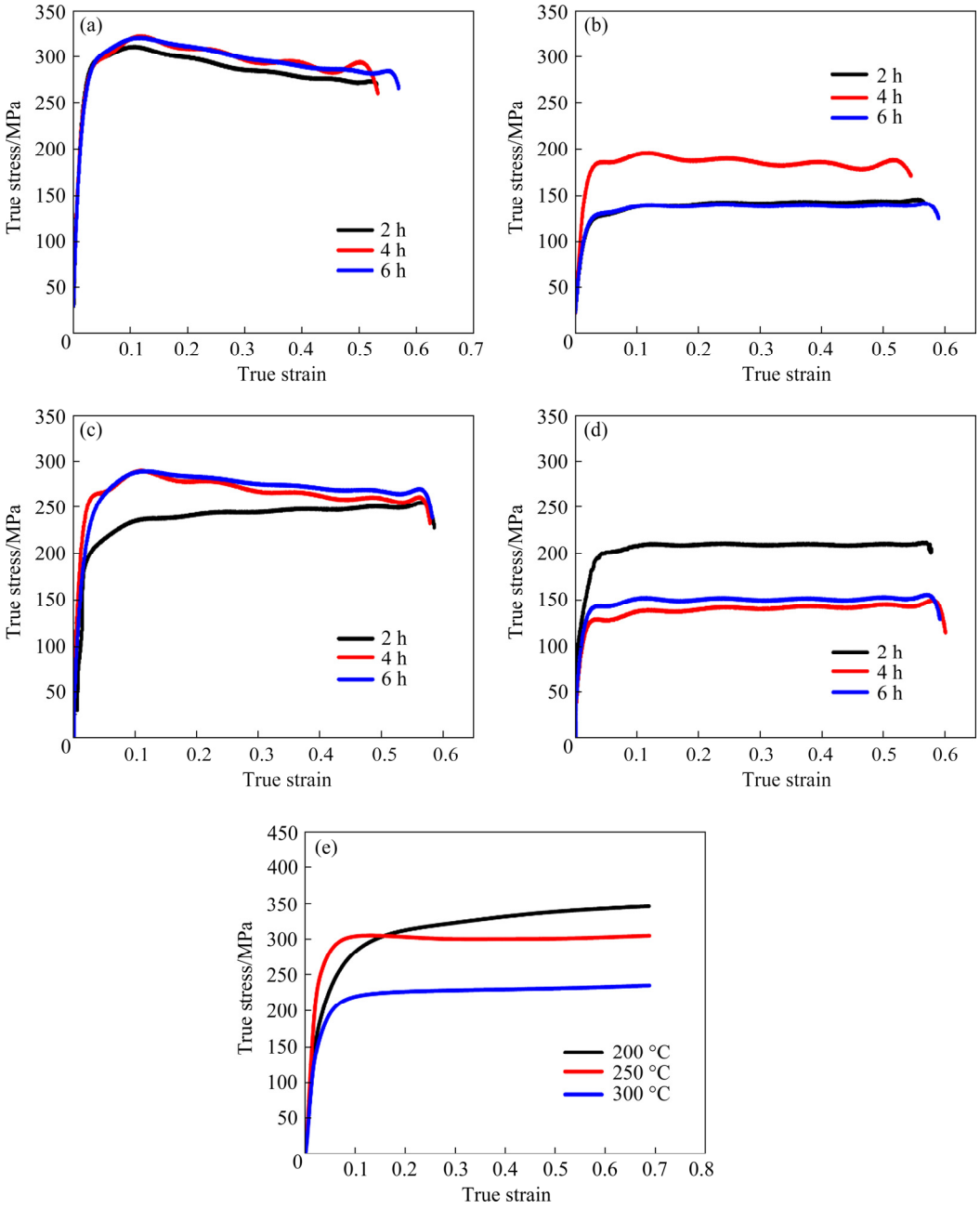

Fig. 4 True strain−stress curves of different samples: (a) 200 °C, 10 min; (b) 250 °C, 10 min; (c) 200 °C, 5 min; (d) 250 °C, 5 min; (e) T4-treated

3.2 Mechanical properties after deformation

Figure 5 shows the Vickers hardness values of samples formed after different heat treatments, and the Vickers hardness value of samples after pretreatment without deformation is also marked in Fig. 5. When different pretreated samples are formed at 200 °C, the hardness of the samples increases with the prolongation of the presaging time, regardless of whether the holding time is 5 or 10 min. The hardness of the sample preaged at 120 °C is higher than that of the T4-treated sample. The maximum hardness is HV 130 when preaging for 6 h and holding at 200 °C for 10 min. The result shows that there is no obvious correlation for the hardness of samples under different pretreatments when formed at 250 °C. The hardness of the samples after being held for 5 and 10 min at 250 °C is not significantly different. Compared with the samples formed at 200 °C, the hardness of the samples decreases significantly, and the hardness is between HV 80 and HV 90. Compared with the pretreated samples, the hardness of the samples formed at 200 °C significantly increases, while the hardness of the samples formed at 250 °C decreases.

According to the comparison of hardness and tensile strength, the tensile strength also presents the same varying tendency.

3.3 Microstructure after deformation

Figure 6 shows the grain structure of each sample under an optical microscope (OM). By

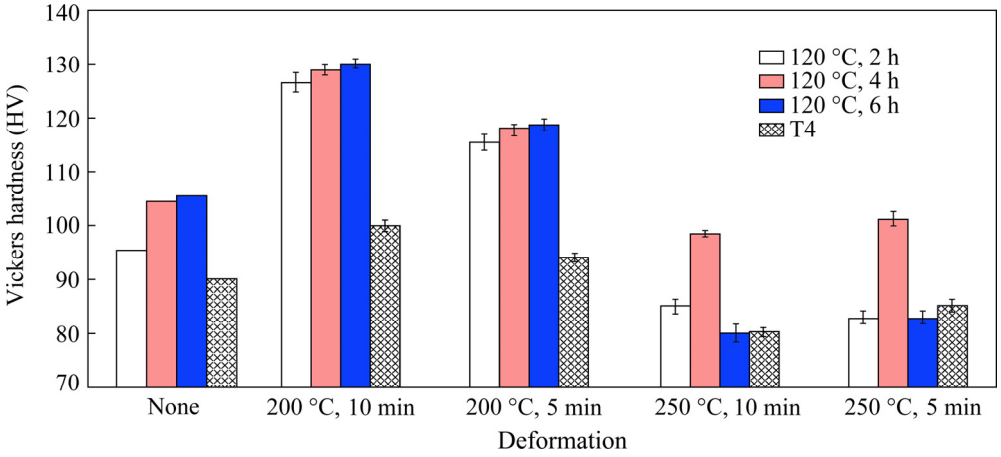

Fig. 5 Vickers hardness of samples

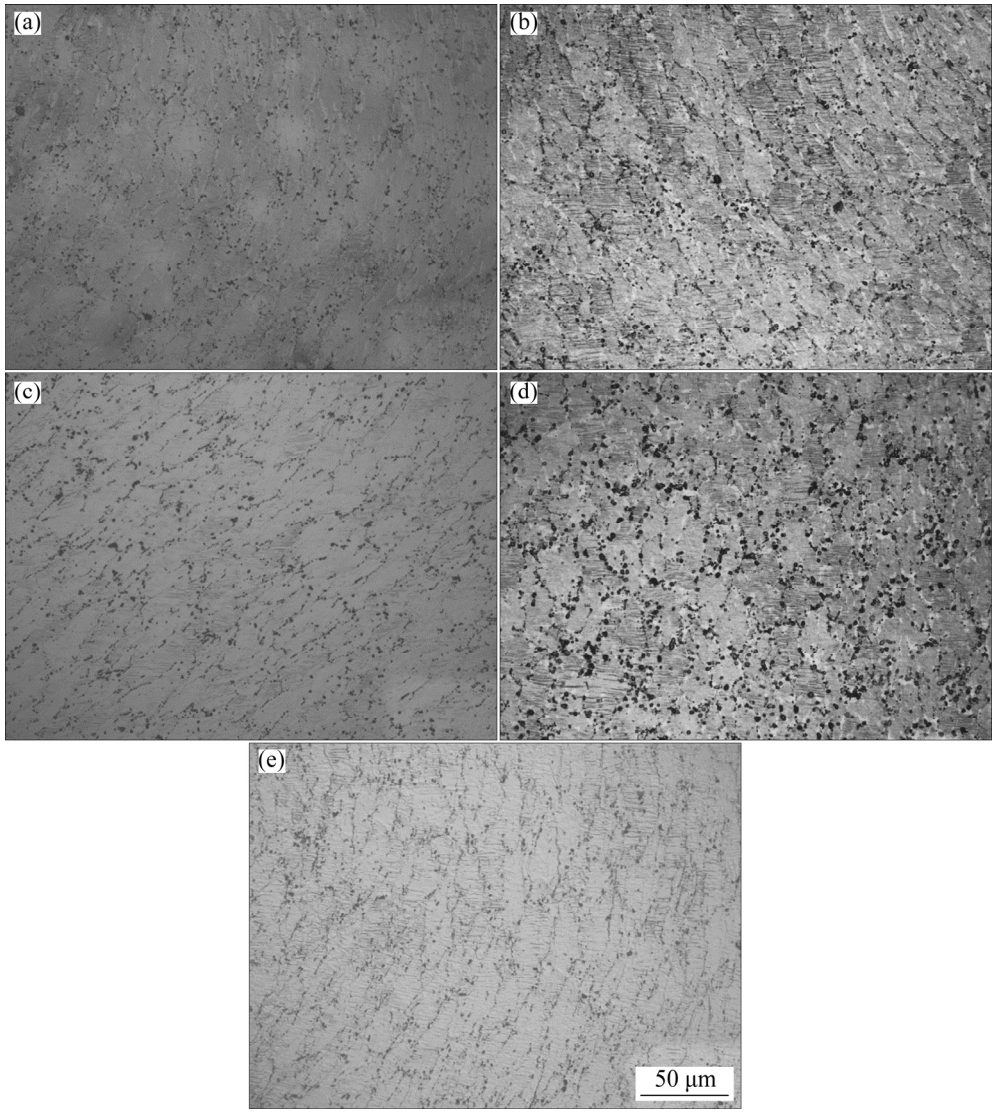

Fig. 6 Microstructures of samples under OM: (a) 120 °C, 2 h + 200 °C, 10 min; (b) 120 °C, 4 h + 200 °C, 10 min; (c) 120 °C, 6 h + 200 °C, 10 min; (d) 120 °C, 4 h + 200 °C, 5 min; (e) 120 °C, 6 h + 250 °C, 10 min

comparing the samples aged at 120 °C for 2, 4 and 6 h (Figs. 6(a, b and c)), the samples with forming temperatures of 200 and 250 °C (Figs. 6(c, e)), and the samples with different holding time of 5 and 10 min (Figs. 6(b, d)), it can be observed that there is no obvious difference in the grain size of the samples. It can also be concluded that the grain size of samples aged at 120 °C for 2, 4 and 6 h shows almost no difference. Similarly, the grain size of samples formed at 200 and 250 °C shows nearly no difference, and holding for 5 or 10 min practically has no effect on the grain size.

3.4 Forging process parameters

According to Fig. 5, when the deformation temperature is 200 °C, the hardness is apparently higher than that when the deformation temperature is 250 °C, and the hardness increases with increasing preaging time and holding time. According to Fig. 4, the plasticity at 250 °C is better than that at 200 °C. However, due to the small amount of deformation of the final forging, the required compression force is low, and the forming temperature and holding time can be selected as 200 °C and 10 min. By comparing the mechanical properties of the compressed samples after preaging at 120 °C for different time and T4 treatment, it is found that when forming at 200 °C, the preaging time has little effect on the hardness. Combined with the properties and energy consumption, the preaging time should be 4 h. In general, the forging process parameters should be as follows: preaging at 120 °C for 4 h and then holding at 200 °C for 10 min.

From the research results, it can be concluded that the new process of short-term heat preservation after preaging can ensure good formability and mechanical properties after forging of the workpiece. Therefore, the new process and its best parameters are determined. First, the billet is subjected to solid solution treatment at 535 °C, followed by upsetting, flattening, and preforging at the solid solution temperature. After that, the workpiece is preaged at 120 °C for 4 h. Finally, the workpiece is kept at 200 °C for 10 min and transferred to the final forging die for final forging, as shown in Fig. 7(a). The mechanical properties of the workpieces obtained by the new process are significantly improved compared with those of the workpieces obtained by the traditional process (Fig. 7(b)). Meanwhile, the final forging die is preheated to 200 °C to ensure that the temperature of the contact surface does not drop greatly, thus improving the formability and mechanical properties. Compared with the traditional process, the process segments are decreased by approximately 40% by reducing the operation time from 10 to 6 h.

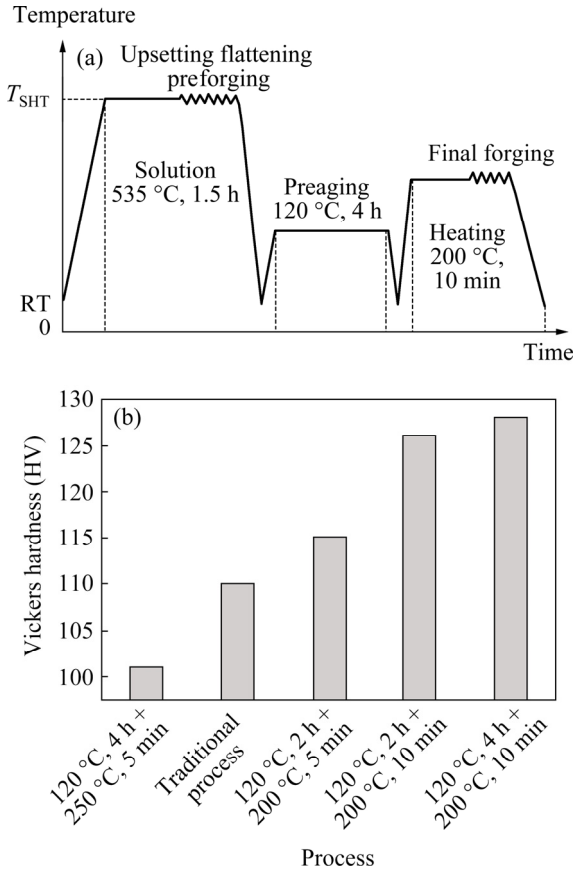

Fig. 7 New forging process (a) and comparison with traditional process in mechanical property (b)

4 Discussion

4.1 Effect of grain boundary strengthening and dislocation strengthening

To explore the reasons for the differences in the mechanical properties of the samples, the effect of grain boundary strengthening on the mechanical properties was considered. The strength provided by grain boundary strengthening can be calculated by the Hall−Petch equation [14,15]:

$$\sigma_y = \sigma_0 + kd^{-1/2} \quad (1)$$

where k is a constant related to the material and d is the average diameter of the grain. According to Eq. (1), grain boundary strengthening is only

related to the average diameter of the grain. Figure 6 shows that there is no obvious difference in the grain size of each sample, and the strengths of the samples provided by σ_y are almost identical.

Figure 8 shows the dislocation of samples at 200 and 250 °C under bright-field TEM. Figure 8(a) shows the sample aged for 6 h and formed after being held at 200 °C for 10 min. A large number of dislocations are formed after the samples are compressed at low temperature. When the deformation temperature is 200 °C, the dynamic recovery is relatively slow, and the dislocations cannot be eliminated in time, resulting in dislocation accumulation. When the deformation temperature is 250 °C, as shown in Fig. 8(b), the increase in temperature accelerates the dynamic recovery, and then the dislocation density is reduced. The strength provided by dislocation strengthening can be expressed by the following equation [16]:

$$\sigma_d = M\alpha Gb\sqrt{\rho} \quad (2)$$

where b is the magnitude of Burgers vector, G is the shear modulus, α is a constant close to 0.5, and M is the Taylor factor. In Fig. 8, the dislocation density of the sample at 200 °C is relatively high, so the strength provided by the dislocation is higher, which is also a factor of the better mechanical properties of the sample.

4.2 Effect of precipitation strengthening with different temperatures and time

The mechanical properties of Al−Mg−Si alloys can be improved by obtaining dispersed nanoscale precipitates during aging treatment [17]. A large number of studies [18−20] have revealed that the structure and size of precipitates play the main role in the variation in the strength of Al−Mg−Si alloys. Figure 9 shows the bright-field TEM morphologies

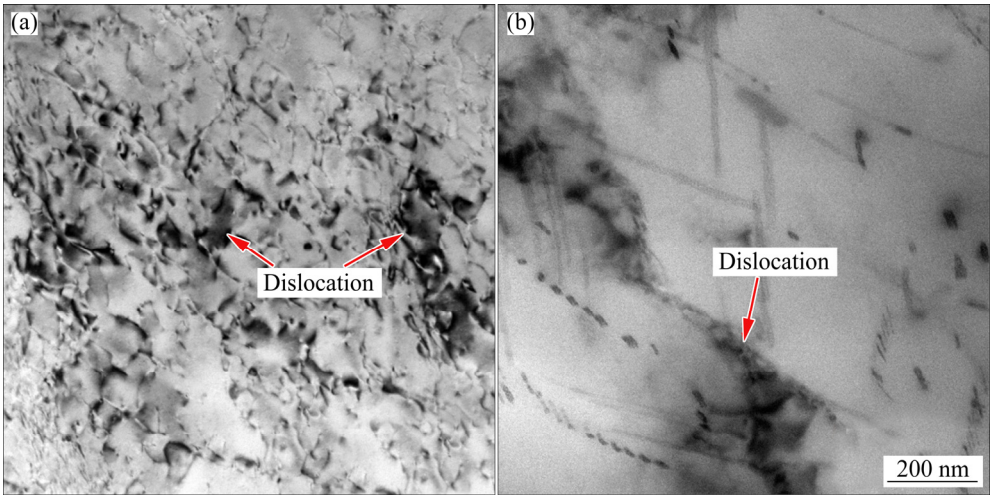

Fig. 8 Dislocation distribution under bright-field TEM: (a) 120 °C, 6 h + 200 °C, 10 min; (b) 120 °C, 6 h + 250 °C, 10 min

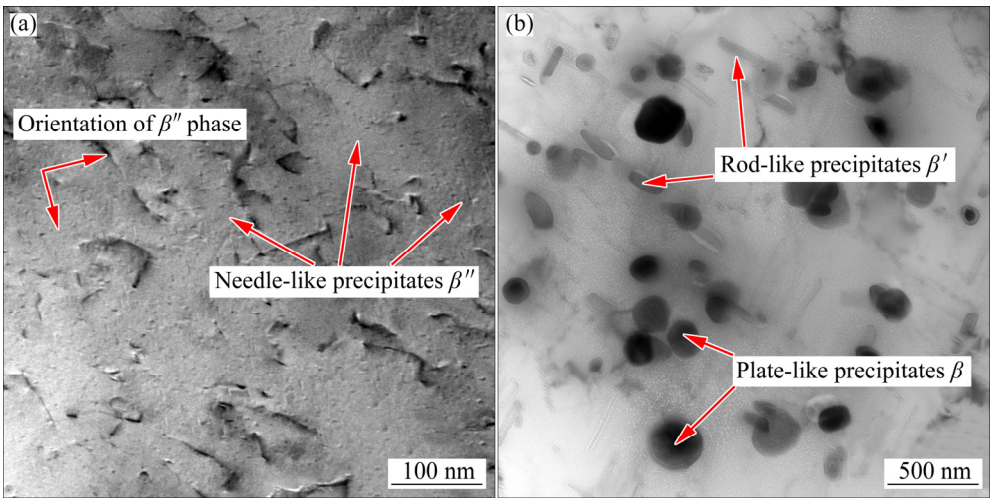

Fig. 9 TEM morphologies of precipitate phases: (a) 120 °C, 6 h + 200 °C, 10 min; (b) 120 °C, 6 h + 250 °C, 10 min

of the samples preaged at 120 °C for 6 h and then formed after being held at 200 and 250 °C for 10 min. A large number of needle-like β'' phases precipitate in the sample formed at 200 °C (Fig. 9(a)), and the β'' phase is the main precipitate, while the β' phase and β phase hardly appear. However, in the sample formed at 250 °C (Fig. 9(b)), there exist mainly rod-like β' phases and plate-like β phases. The Vickers hardness of the 120 °C, 6 h + 200 °C, 10 min sample is HV 130, while that of the 120 °C, 6 h + 250 °C, 10 min sample is only HV 80. We can conclude that the structure and size of precipitates have a great influence on the hardness.

Figure 10 shows the SEM images of samples preaged at 120 °C for 6 h, held at 200 °C for 5 and 10 min, and held at 250 °C for 10 min. Figure 10(b) shows EDS analysis results of the 120 °C, 6 h + 200 °C, 10 min sample. It can be seen that the large white spot contains a large amount of Fe and Mn, while the main strengthening precipitates are Mg and Si compounds. Therefore, it can be judged that the large white spots are the insoluble phase without a strengthening effect; in contrast, the small white spots are the strengthening precipitates. In the 120 °C, 6 h + 200 °C, 10 min sample (Fig. 10(a)), the strengthening precipitates are the most abundant, so it has the highest strength. When the temperature increases to 250 °C (Fig. 10(c)), strengthening precipitate phases are rarely observed, resulting in a decrease in strength. Similarly, when the holding time is shortened to 5 min (Fig. 10(d)), the strengthening precipitate phases are also reduced compared to the 120 °C, 6 h + 200 °C, 10 min sample, and its strength also decreases.

Many studies [21−23] indicate that the strength contributed by precipitates in Al−Mg−Si alloys can be expressed as

$$\sigma_{\mathrm{p}}=\frac{M}{b\bar{r}}\left(2\beta Gb^{2}\right)^{-1/2}\left(\frac{3f}{2\pi}\right)^{1/2}\bar{F}^{3/2} \tag{3}$$

where $\bar{F}$ is the mean obstacle strength, $\bar{r}$ is the mean particle size, f is the volume fraction, and β is a constant of approximately 0.5. According to Eq. (3), the strength provided by the precipitate is low when the size of the precipitate is large. In addition, the larger the volume fraction (f) of the precipitate is, the greater the proportion of strength it can provide. Many studies [24−27] show that the precipitation order of Al−Mg−Si alloys is as follows:

Clusters of Si atoms → GP I zones → GP II zones/β'' → β' → β

Among these precipitates, the β'' phase has the minimum size, which is the best strengthening precipitate in the Al−Mg−Si alloy. The greater the amount of β'' phase is, the higher the strength of the workpiece [28,29].

According to Fig. 9(a), most of the precipitates in the 120 °C, 6 h + 200 °C, 10 min sample are β''

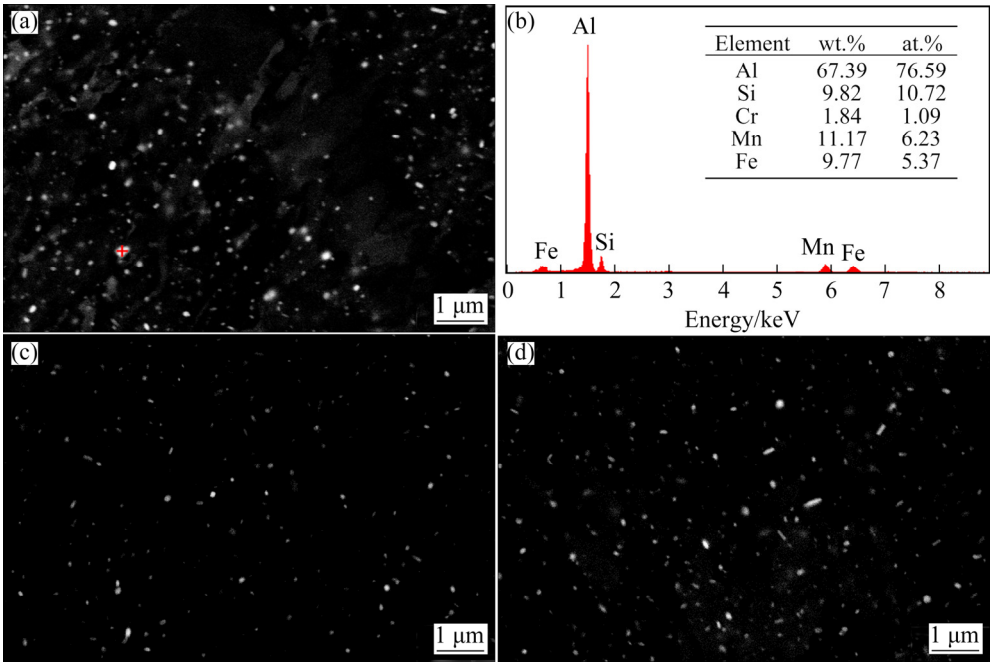

Fig. 10 SEM morphologies of samples and EDS analysis result: (a, b) 120 °C, 6 h + 200 °C, 10 min; (c) 120 °C, 6 h + 250 °C, 10 min; (d) 120 °C, 6 h + 200 °C, 5 min

phases, and Fig. 10(b) shows that the distribution of precipitates is very dense, so the strength of the sample is the highest, while most of the precipitates in the 120 °C, 6 h + 250 °C, 10 min sample (Fig. 9(b)) are transformed into β' and β phases, and Fig. 10(c) shows that the density of precipitates is low, so the strength is poor.

Figure 11(a) shows the DSC curve of 6082 aluminum alloy after solid solution treatment. There are four exothermic peaks of 6082 aluminum alloy after solid solution treatment. Peak 1 is located at approximately 100 °C, which is considered to be the formation of the GP zone. The second exothermic Peak 2 is located at approximately 235 °C, which is considered the precipitation peak of the β'' phase. At this temperature, the precipitates transform into the β'' phases. With a further increase in temperature, the precipitates in the alloy continue to transform. When the temperature reaches approximately 300−320 °C, the third exothermic Peak 3 appears on the curve, which is the precipitation peak of the β' phase. Peak 4 appears when the temperature reaches 450 °C, and the precipitates transform into the stable β phase, which is Mg_2Si [30−32]. According to Fig. 5, the hardness of samples preaged for 2, 4 and 6 h shows little difference. Combined with Fig. 11(b), the first peak of the DSC curve after aging disappears, which indicates that the GP zone is completely precipitated after aging at 120 °C for 2 h. The height of Peak 2 decreases with the increase of aging time, which indicates that the transformation from the GP zone to the β'' phase is more thorough with the increase of aging time. The heights of Peak 3 and Peak 4 are similar to those for the sample after solid solution treatment, indicating that the precipitates do not transform into β' and β during aging at 120 °C. On the DSC curve of the T4-treated sample, only Peak 1 disappears, and the heights of Peaks 2, 3, and 4 are almost the same as those of the solid solution sample, which indicates that the precipitation of the GP zone only occurs during natural aging, and the does not transform into β''.

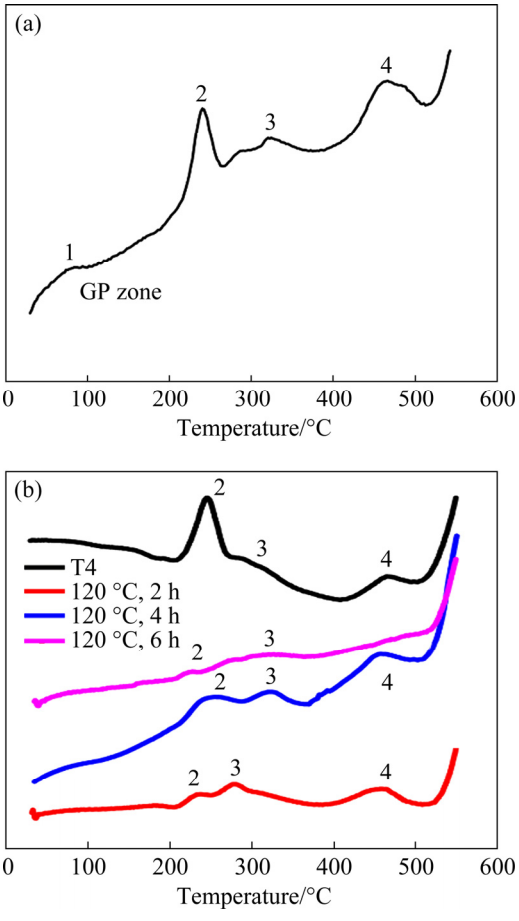

Fig. 11 DSC curves of 6082 aluminum alloy after solid solution treatment (a) and samples after different aging treatments (b)

5 Conclusions

(1) A new forging process of 6082 aluminum alloy with high efficiency and energy savings is proposed: solid solution treatment + preforging + short time preaging + final forging. The sample formed after aging at 120 °C for 4−6 h and holding at 200 °C for 10 min has the best mechanical properties, and the Vickers hardness of the workpiece is HV 20 higher than that obtained from the traditional process.

(2) The Vickers hardness of the samples formed at 200 °C is higher than that at 250 °C. When the samples are formed at 200 °C, the sample preaged for 6 h and held for 10 min before forming has the highest Vickers hardness with a value of HV 130.

(3) In this forging process, the strength of workpieces that are finally-forged at 200 °C is effectively improved by dislocation strengthening and precipitation strengthening. Extensively distributed β'' phases are observed accompanied by dislocations in workpieces that are finally-forged at 200 °C, especially in workpieces that are finally-forged after being held at 200 °C for 10 min.

Acknowledgments

This work is financially supported by the

National Natural Science Foundation of China (Nos. 51775397, 52075400), “111” Project of China (No. B17034), the Major Program of Science and Technology Program of Hubei Province, China (Nos. 2019AAA007, 2020BAB140), and the Innovative Research Team Development Program of Ministry of Education of China (No. IRT17R83).

References

[1] BIROL Y, AKDI S. Cooling slope casting to produce EN AW 6082 forging stock for manufacture of suspension components [J]. Transactions of Nonferrous Metals Society of China, 2014, 24: 1674−1682.

[2] LI Hong-ying, ZENG Cui-ting, HAN Mao-sheng, LIU Jiao-jiao, LU Xiao-chao. Time−temperature−property curves for quench sensitivity of 6063 aluminum alloy [J]. Transactions of Nonferrous Metals Society of China, 2013, 23: 38−45.

[3] SUN Wen-long, CHEN Xiao-kai, WANG Lu. Analysis of energy saving and emission reduction of vehicles using light weight materials [J]. Energy Procedia, 2016, 88: 889−893.

[4] BIROL Y, GOKCIL E, AKDI S. Potential of twin-belt-cast EN AW 6082 blanks for the manufacture of wishbone suspension forgings [J]. International Journal of Advanced Manufacturing Technology, 2017, 92: 3693−3701.

[5] BIROL Y, ILGAZ O. Effect of cast and extruded stock on grain structure of EN AW 6082 alloy forgings [J]. Materials Science and Technology, 2014, 30: 860−866.

[6] BIROL Y, GOKCIL E, GUVENC M A, AKDI S. Processing of high strength EN AW 6082 forgings without a solution heat treatment [J]. Materials Science and Engineering A, 2016, 674: 25−32.

[7] DIN S U, KAMRAN J, HASAN B A, TARIQ N H, MEHMOOD M, ZUHA M. Effect of thermo mechanical treatments and aging parameters on mechanical properties of Al−Mg−Si alloy containing 3 wt.% Li [J]. Materials and Design, 2014, 64: 366−373.

[8] LIU R, TIAN Y Z, ZHANG Z J, ZHANG P, ZHANG Z F. Fatigue strength plateau induced by microstructure inhomogeneity [J]. Materials Science and Engineering A, 2017, 702: 259−264.

[9] KUMAR N, OWOLABI G M, JAYAGANTHAN R, AJIDE O O, SONKER S, WARNER G. Hot-compression response of solution-treated Al−Mg−Si alloy [J]. Journal of Materials Engineering and Performance, 2019, 28: 7602−7615.

[10] SI Jia-yong, HAN Peng-biao, CHANG Xia, ZHANG Ji. Flow behavior of Ti−46.2Al−2.5V−1.0Cr−0.3Ni alloy in secondary hot deformation [J]. Transactions of Nonferrous Metals Society of China, 2006, 16: s2091−s2095.

[11] BABANIARIS S, RAMAJAYAM M, JIANG Lu, VARMA R, LANGAN T, DORIN T. Effect of Al−3(Sc,Zr) dispersoids on the hot deformation behavior of 6xxx-series alloys: A physically based constitutive model [J]. Materials Science and Engineering A, 2020, 793: 139873.

[12] KUMAR N, JAYAGANTHAN R, BROKMEIER H G. Effect of deformation temperature on precipitation, microstructural evolution, mechanical and corrosion behavior of 6082 Al alloy [J]. Transactions of Nonferrous Metals Society of China, 2017, 27: 475−492.

[13] LI Kuo, PAN Qing-lin, LI Rui-shi, LIU Shu-hui, HUANG Zhi-qi, HE Xin. Constitutive modeling of the hot deformation behavior in 6082 aluminum alloy [J]. Journal of Materials Engineering and Performance, 2019, 28: 981−994.

[14] JIA Hai-long, BJORGE R, CAO Ling-fei, SONG Hui, MARTHNSEN K, LI Yan-jun. Quantifying the grain boundary segregation strengthening induced by post-ECAP aging in an Al−5Cu alloy [J]. Acta Materialia, 2018, 155: 199−213.

[15] ZHANG Wen-pei, LI Huan-huan, HU Zhi-li, HUA Lin. Investigation on the deformation behavior and post-formed microstructure/properties of AA7075-T6 alloy under pre-hardened hot forming process [J]. Materials Science and Engineering A, 2020, 792: 139749.

[16] ENGLER O, MARIOARA C D, ARUGA Y, KOZUKA M, MYHR O R. Effect of natural ageing or pre-ageing on the evolution of precipitate structure and strength during age hardening of Al−Mg−Si alloy AA 6016 [J]. Materials Science and Engineering A, 2019, 759: 520−529.

[17] ZHAO Tian-sheng, ZHOU Jie, ZHOU Jun-feng, WU Dao-xiang, XIONG Yu. Influence of pre-stretching and aging processes on comprehensive performance of aluminum alloy [J]. Materials and Manufacturing Processes, 2018, 33: 1641−1647.

[18] MARIOARA C D, ANDERSEN S J, JANSEN J, ZANDBERGEN H W. Atomic model for GP-zones in a 6082 Al−Mg−Si system [J]. Acta Materialia, 2001, 49: 321−328.

[19] ANDERSEN S J, ZANDBERGEN H W, JANSEN J. The crystal structure of the β'' phase in Al−Mg−Si alloys [J]. Acta Materialia, 1998, 46: 3283−3298.

[20] ZANDBERGEN H W, ANDERSEN S J, JANSEN J. Structure determination of Mg_5Si_6 particles in Al by dymamic electron diffraction studies [J]. Science, 1997, 277: 1221−1225.

[21] LI Y L, KOHAR C P, MISHRA R K, INAL K. A new crystal plasticity constitutive model for simulating precipitation-hardenable aluminum alloys [J]. International Journal of Plasticity, 2020, 132: 102759.

[22] MYHR O R, GRONG O, ANDERSEN S J. Modelling of the age hardening behavior of Al−Mg−Si alloys [J]. Acta Materialia, 2001, 49: 65−75.

[23] NOURI S, KAZEMINEZHAD M, SHADKAM A. Flow stress of 2024 aluminum alloy during multi-directional forging process and natural aging after plastic deformation [J]. Materials Chemistry and Physics, 2020, 254: 123446.

[24] LAI Y X, JIANG B C, LIU C H, CHEN Z K, WU C L, CHEN J H. Low-alloy-correlated reversal of the precipitation sequence in Al−Mg−Si alloys [J]. Journal of Alloys and Compounds, 2017, 701: 94−98.

[25] NEMOUR H, IBRAHIM D M, TRIKI A. The effect of heavy cold plastic deformation on the non-isothermal kinetics and the precipitation sequence of metastable phases in an Al−Mg−Si alloy [J]. Journal of Thermal Analysis and Calorimetry, 2016, 123: 1−8.

[26] WANG Xiang, ESMAEILI S, LLOYD D J. The sequence of

precipitation in the Al−Mg−Si−Cu alloy AA6111 [J]. Metallurgical and Materials Transactions A, 2006, 37: 2691−2699.

[27] YASSAR R S, FIELD D P, WEILAND H. Transmission electron microscopy and differential scanning calorimetry studies on the precipitation sequence in an Al−Mg−Si alloy: AA6022 [J]. Journal of Materials Research, 2005, 20: 2705−2711.

[28] LAI Y X, FAN W, YIN M J, WU C L, CHEN J H. Structures and formation mechanisms of dislocation-induced precipitates in relation to the age-hardening responses of Al−Mg−Si alloys [J]. Journal of Materials Science and Technology, 2020, 41: 127−138.

[29] WANG Xiang-dong, LIU Xiong, DING Hao, YAN Su-rong, XIE Zi-hua, PAN Bai-qing, LI Yong-hong, PAN Qing-lin, DENG Yun-lai, WANG Wei-yi. Microstructure and mechanical properties of Al−Mg−Si alloy U-shaped profile [J]. Transactions of Nonferrous Metals Society of China, 2020, 30: 2915−2926.

[30] DJEMA O, BOUABDALLAH M, BADJI R, SAADI A, KHERROUBA N, SAHLI A. Isothermal and non-isothermal precipitation kinetics in Al−Mg−Si−(Ag) alloy [J]. Materials Chemistry and Physics, 2020, 240: 122073.

[31] CHEN Zhi-xing, LIU Kun, ELGALLAD E, BRETON F, CHEN X G. Differential scanning calorimetry fingerprints of various heat-treatment tempers of different aluminum alloys [J]. Metals, 2020, 10: 763.

[32] GAO Guan-jun, HE Chen, LI Yong, LI Jia-dong, WANG Zhao-dong, MISRA R D K. Influence of different solution methods on microstructure, precipitation behavior and mechanical properties of Al−Mg−Si alloy [J]. Transactions of Nonferrous Metals Society of China, 2018, 28: 839−847.

预时效热锻工艺处理 6082 铝合金的显微组织和力学性能

华 林[1,2,3,4]，袁普光[1,2]，赵 宁[1,2]，胡志力[1,2,3,4]，马慧娟[1,2]

1. 武汉理工大学 现代汽车零部件技术湖北省重点实验室，武汉 430070；
2. 武汉理工大学 汽车零部件技术湖北省协同创新中心，武汉 430070；
3. 武汉理工大学 新能源与智能网联汽车湖北省工程技术中心，武汉 430070；
4. 武汉理工大学 材料绿色精密成形技术与装备湖北省工程研究中心，武汉 430070

摘 要：提出一种新的 6082 铝合金锻造工艺，该工艺在保证力学性能的同时可节约时间、降低能耗。该工艺将坯料在固溶温度进行预锻，然后进行预时效，最终在 200 ℃进行终锻。通过热压缩实验研究预时效后的压缩行为和力学性能，通过 SEM、TEM 和 DSC 研究不同工艺参数下试样的析出相差异。研究发现在 120 ℃预时效 4 h，并在 200 ℃保温 10 min 的材料具有最佳综合性能，锻件维氏硬度为 HV 128，比传统工艺锻件的高。在 200 ℃下终锻时，材料在析出强化和位错强化提升较大。该锻造工艺具有耗时短、能耗低的优势，能在保证强度达标的前提下有效提高生产效率。

关键词：6082 铝合金；锻造；预时效；压缩行为；硬度；析出相

(Edited by Bing YANG)